



Joint angle and delay estimation for GNSS multipath signals based on multiple sparse Bayesian Learning

Ning Chang¹ · Wenjie Wang¹ · Xi Hong¹ · José A. López-Salcedo² · Gonzalo Seco-Granados²

Received: 3 April 2020 / Accepted: 15 December 2020

© The Author(s), under exclusive licence to Springer-Verlag GmbH, DE part of Springer Nature 2021

Abstract

Multipath signals formed by signal reflection coming from objects in the vicinity of Global Navigation Satellite System (GNSS) receivers result in a degradation of the tracking performance and an increase in the positioning error. By estimating the parameters of both line-of-sight signal and the multipath signals, superior multipath mitigation, spoofing suppression, and localization can be attained. We propose using the multiple sparse Bayesian learning method together with the joint angle and delay estimation technique in GNSS multipath environment to fully exploit the sparsity present in both the spatial and the temporal domains. We also extend the techniques to the estimation of fractional Doppler frequency besides the angle and delay. To counteract the intrinsic drawbacks of sparse representations, two different algorithms based on on-grid and off-grid estimators are proposed to either reduce the complexity or enhance the resolution such that the proposed multipath mitigation approach can be adapted to various GNSS practical situations. Subsequently, a third algorithm with improved resolution is obtained by applying the Space Alternating Generalized Expectation–Maximization algorithm to refine the MSBL-based joint angle and delay estimates. Simulation results indicate that the three proposed algorithms can effectively resolve the GNSS multipath signals and have better performance than existing methods even in severe situations, like the cases of signals with low carrier-to-noise-power-density ratio and spatially and temporally correlated multipath.

Keywords GNSS multipath signals · Multiple sparse Bayesian learning · Joint angle and delay estimate · Off-grid estimation

Introduction

The GNSS acronym generally refers to diverse Global Satellite Navigation Systems such as GPS, Galileo and Beidou, and their augmentation systems. GNSS can provide accurate position, velocity and time to users, but it is vulnerable to a variety of propagation effects. Multipath propagation is often the dominant error source in GNSS, and it may cause significant tracking performance degradation and positioning error increase (Van Nee 1992). In particular, the pseudo-range error produced by multipath can reach meters or even hundreds of meters in traditional GNSS receivers (Kalyanaraman et al. 2006; Kos et al. 2010) posing a serious concern to the system accuracy and reliability.

Multi-antenna GNSS receivers combat the multipath problem in the spatial domain (Maqsood et al. 2010), which provides the required degrees of freedom for direction-of-arrival (DOA) estimation and multipath separation or cancelation. Due to a significant leap forward in radio frequency and antenna implementations, significant research and development efforts have been devoted to estimating multipath parameters in GNSS utilizing multi-antenna receivers. Many methods may be classified as either maximum likelihood-based and subspace-based approaches. Referring to the former, the most classical yet the most used method is the maximum likelihood (ML) estimator (Seco Granados 2000; Seco Granados et al. 2005). Stemming from the ML, the RELAXation algorithm (Li et al. 1997; Jia et al. 2017) is proposed to estimate angle and waveform iteratively. Later, the interesting Space Alternating Generalized Expectation–Maximization (SAGE) approach (Fleury et al. 1999; Antreich et al. 2008, 2011) was also proposed for the multipath estimation problem. Most of these methods provide a good estimation performance but require a

✉ Ning Chang
changning@stu.xjtu.edu.cn

¹ Xi'an Jiaotong University, Xi'an, People's Republic of China

² Universitat Autònoma de Barcelona, Barcelona, Spain

compromise between performance and complexity. Besides the ML-based approaches, the other type of methods are the subspace-based approaches, which rely on decomposing the signal into the signal and noise subspaces. Some examples are the multiple signal classification (MUSIC) method (Schmidt 1986) and the estimating signal parameters via rotational invariance (ESPRIT) (Roy and Kailath 1989) method. While they are suboptimal in general, they are less computationally intensive than the ML-based approaches. In order to tackle the limitations of subspace-based approaches with coherent signals, the forward–backward averaging and spatial smoothing methods (Pillai and Kwon 1989) have been used. To further increase the discrimination, the joint angle and delay estimation method (JADE) (Vanderveen et al. 1997; Veen et al. 1998; Chang et al. 2018; Hong et al. 2018) has been proposed to obtain the parameters by using a collection of estimates of the space–time channel. However, it is important to point out that most of these methods cannot work well in the case of highly correlated multipath (Fleury et al. 1999; Misra and Enge 2011). This case refers to the situation where the delay difference of these impinging rays is smaller than half a chip or their angle difference is smaller than the array beamwidth. Moreover, such methods still suffer degradation when fewer snapshots, lower C/N_0 as well as incompletely compensated Doppler frequency offsets (DFO) existed in the situation.

Besides the methods above, an alternative approach obtained by formulating the problem using sparsity (Fortunati et al. 2014; Gerstoft et al. 2016) gained noticeable interest recently. For instance, convex optimization methods such as the least absolute shrinkage and selection operator (Tibshirani 1996) or the basis pursuit algorithm (Chen et al. 2001) are effective once the signal representation is sufficiently sparse. Alternatively, the iterative adaptive (IAA) method (Du et al. 2009) and the IAA apply amplitude and phase estimation (Yardibi et al. 2010) and update the spatial power estimates and weighting vectors based on weighted least squares algorithm. Furthermore, the sparse Bayesian learning (SBL) (Tipping 2001) and its extension, the multi-snapshot SBL (MSBL) (Wipf and Rao 2007), use a Bayesian rule together with the expectation–maximization iteration to eliminate the user parameters. The attractive points of SBL (Zhang and Rao 2001) are that its global minima are always the sparsest ones and it has few local minima. Although SBL-based methods have a lot of benefits, the on-grid estimation leads to the off-grid effects that most of the true parameters do not strictly fall onto the grid point (Fortunati et al. 2014). The bias between the real value and the nearest grid tends to zero only as the number of the grid points tends to infinity and vice versa, but the number of grid points cannot be arbitrarily increased for the sake of computational cost. To significantly improve the DOA estimation performance without dense sampling grids, the

off-grid DOA estimation method (Zhu et al. 2011) and off-grid sparse Bayesian inference (OGSBI) (Yang et al. 2012) method have been proposed. Also, the perturbed MSBL-based algorithm (Chen et al. 2018) has been put forward to solve the DOA estimation problem with a mutual coupling matrix.

Although the joint angle and delay estimation MSBL-based methods (JADE-MSBL) are appropriate for solving the multipath discrimination problem and enhancing parameter estimation accuracy, such methods still face an important limitation in practical GNSS environments. More specifically, if more precise parameter estimation is needed, JADE-MSBL methods result in a highly correlated matrix and huge complexity as a result of using dense sampling grids introduced by the joint on-grid estimation. In addition, different joint DOA and delay estimation algorithms are considered to satisfy the various implementation and accuracy needs of practical GNSS receiver. For example, the quality of GNSS pseudo-range observable stems directly from the accuracy of the delay estimate rather than from the DOA estimate, but on the other hand, accurate DOA estimates are crucial in the implementation of multipath mitigation via spatial filtering. The different preferences and trade-offs between the accuracy of the DOA and delay estimates have not been comprehensively considered in previous works.

Inspired by the robustness against multipath of MSBL and the required accuracy of the different GNSS parameters, three new methods for the joint DOA and delay estimation problem for GNSS multipath signals are proposed. First, we formulate the spatial–temporal sparse models. Second, the MSBL algorithm is derived to jointly estimate DOA and delay and achieve improved robustness against multipath, adaptiveness to low C/N_0 values and ability to work with a small number of snapshots. Combinations of the on-grid and off-grid MSBL estimation, with a possibly different treatment of the spatial and temporal domains, are particularly designed to greatly reduce the computational overhead or accurately estimate parameters. Third, considering several practical GNSS situations, three algorithms are presented to meet the various performance requirements. The algorithm for joint on-grid DOA and off-grid delay MSBL estimation (JAODE-MSBL) is proposed for the situation where the delay is to be more accurately estimated than the DOA. We put forward the joint off-grid DOA and on-grid delay MSBL estimation (JOADE-MSBL) algorithm for the reverse case. Additionally, the SAGE is a viable option for further refining the results of JADE-MSBL to obtain both precise DOA and delay, resulting in the method called JADE-MSBL&SAGE. Finally, we compare the three proposed algorithms in many aspects with the state-of-the-art methods to prove their ability to resolve the multipath signals and the superiority in parameter estimation, especially in some severe multipath conditions for GNSS receiver.

Notations: Matrices are denoted by capital letters in boldface (e.g., \mathbf{A}), and vectors are denoted by lowercase letters in boldface (e.g., \mathbf{a}). $\mathbb{C}^{M \times N}$ denotes the set of $M \times N$ matrices with the entries being complex numbers. $\mathbf{I}_N \in \mathbb{C}^{N \times N}$ denotes an identity matrix. $E\{\cdot\}$ denotes the expectation operation. $\mathcal{CN}(\boldsymbol{\mu}, \boldsymbol{\Sigma})$ denotes the complex Gaussian distribution with the mean being $\boldsymbol{\mu}$ and the variance matrix being $\boldsymbol{\Sigma}$. $\|\cdot\|_F, \|\cdot\|_2, \otimes, \odot, Tr\{\cdot\}, vec\{\cdot\}, diag\{\cdot\}, (\cdot)^{-1}, (\cdot)^T, (\cdot)^H$ denote the Frobenius norm, the ℓ_2 norm, the Kronecker product, the Hadamard product, the trace of a matrix, the vectorization of a matrix, the diagonalization of a matrix, the inversion, the matrix transpose and the Hermitian transpose, respectively.

Signal model

This section contains two subsections describing two different aspects of the signal model. The first one presents a general spatial-temporal model for GNSS signals in a multipath situation. The second subsection explains how the model can be adapted for a sparse joint spatial and temporal representation.

Joint spatial and temporal data Model for GNSS multipath signals

Without loss of generality, we take the GPS system as our target application system. Consider the wavefield generated by K multipath rays arriving from DOAs $\boldsymbol{\theta}$ with corresponding time delays $\boldsymbol{\tau}$ and DFO \mathbf{v} , where $\boldsymbol{\theta} \doteq [\theta_1, \dots, \theta_K]^T$, $\boldsymbol{\tau} \doteq [\tau_1, \dots, \tau_K]^T$, and $\mathbf{v} \doteq [v_1, \dots, v_K]^T$. Under the narrow-band approximation, the vector $\mathbf{y}(t)$ at the output of an M_θ element array for one specific satellite signal can be expressed as

$$\mathbf{y}(t) = \sum_{k=1}^K \gamma_k \mathbf{a}(\theta_k) c(t - \tau_k) e^{j2\pi v_k t} + \mathbf{e}(t) \tag{1}$$

with $\mathbf{y}(t) \doteq [y_1(t), \dots, y_{M_\theta}(t)]^T$, $\mathbf{a}(\theta_k)$ is the steering vector and γ_k is the amplitude of the k^{th} ray. The term $c(t - \tau_k)$ denotes the C/A code waveform of the k^{th} ray with delay τ_k , and its corresponding DFO is v_k . The Gaussian noise contribution, uncorrelated with the signals, is represented as $\mathbf{e}(t) \doteq [e_1(t), \dots, e_{M_\theta}(t)]^T$. In this context, we assume that number of rays K is already known, and some specific criteria (Akaike 1974; Wax and Kailath 1978) can be applied to determine the number of rays.

Note that the Doppler frequency error is mainly caused by the relative movement between the satellites and receiver, and it can be as large as nearly 5KHz when the GPS signals are impinging the antenna. However, the Doppler differences

of the multipath components among themselves and the line of sight (LOS) are usually small (Irsigler 2010; Xie and Petovello 2015). For a GNSS receiver, the DFO is always coarsely estimated via the signal acquisition (O'Brien 2009; Van Nee and Coenen 1991), and the v_k can be expressed by $v_k \doteq v_c + \delta_k$, $k = 1, \dots, K$, where v_c is the acquired frequency that all the multipath components and the LOS share the same value. δ_k is the residual frequency part which is called fractional Doppler frequency offset (FFO). The received signal with v_c compensated could be represented as

$$\dot{\mathbf{y}}(t) = \sum_{k=1}^K \gamma_k \mathbf{a}(\theta_k) c(t - \tau_k) e^{j2\pi \delta_k t} + \dot{\mathbf{e}}(t) \tag{2}$$

where δ_k is usually constrained in one frequency searching step.

Collecting L samples in each C/A code period, the observed signal during the n^{th} period can be expressed as

$$\mathbf{Y}_b(n) \doteq [\dot{\mathbf{y}}(((n-1)L+1)T_s), \dots, \dot{\mathbf{y}}(((n-1)L+L)T_s)] \tag{3}$$

where T_s is the sample interval and $l = 1, \dots, L$, $n = 1, \dots, N$. Likewise, the sampled shifted waveform $\mathbf{c}(\tau_k)$ and the FFO vector are

$$\mathbf{c}(\tau_k) \doteq [c(T_s - \tau_k), \dots, c(LT_s - \tau_k)]^T \tag{4}$$

$$\mathbf{d}(\delta_k) \doteq [e^{j2\pi \delta_k T_s}, \dots, e^{j2\pi \delta_k L T_s}]^T \tag{5}$$

To obtain the spreading gain and reduce the computational complexity, a transformation matrix to the codespace $\mathbf{B} \doteq [\mathbf{c}(\bar{\tau}_1), \dots, \mathbf{c}(\bar{\tau}_{M_\tau})]^T$ can be applied on each code period. According to the information obtained from the acquisition phase, the set of the uniformly distributed delays $\bar{\boldsymbol{\tau}} \doteq [\bar{\tau}_1, \dots, \bar{\tau}_{M_\tau}]$ is centered on the correlation peak and span both sides, and the number of codebeams satisfies $M_\tau \ll L$. Moreover, vectorization operator spreading in the column is carried out to the temporally beamformed data and we get $\mathbf{y}_s(n) \in \mathbb{C}^{M_\theta M_\tau \times 1}$ as

$$\begin{aligned} \mathbf{y}_s(n) &= vec(\mathbf{Y}_b(n) \cdot \mathbf{B}^H) \\ &= (\mathbf{A}(\boldsymbol{\theta}) \otimes \mathbf{R}(\bar{\boldsymbol{\tau}}, \boldsymbol{\tau}, \boldsymbol{\delta})) \boldsymbol{\gamma}_s + \mathbf{e}_s(n) \end{aligned} \tag{6}$$

with $r(\bar{\tau}_{m_\tau}, \tau_k, \delta_k) \doteq \mathbf{c}^H(\bar{\tau}_{m_\tau})(\mathbf{c}(\tau_k) \odot \mathbf{d}(\delta_k))$, $m_\tau = 1, \dots, M_\tau$, $k = 1, \dots, K$, the element of the matrix $\mathbf{R}(\bar{\boldsymbol{\tau}}, \boldsymbol{\tau}, \boldsymbol{\delta}) \in \mathbb{C}^{M_\tau \times K}$, and the array manifold matrix defined as $\mathbf{A}(\boldsymbol{\theta}) \doteq [\mathbf{a}(\theta_1), \dots, \mathbf{a}(\theta_K)]$. Since FFOs are relatively small compared to DFOs and only have a negligible impact on the DOA and time delay estimation, we assume that FFOs are neglected in following sparse models for the sake of simplicity. Such a simplified model has been widely studied in the existing literature (Seco Granados et al. 2005; Juang 2008;

Fohlmeister et al. 2017). The validity of this FFOs assumption and robustness against FFOs will be comprehensively discussed in Section “Numerical Results.”

Sparse spatial and temporal data model

To exploit the sparsity in both spatial and temporal domains, we extend y_s into a joint two-dimensional spatial and temporal sparse model by using the concept of sparse representation. In addition, we propose three approaches to extend JADE-MSBL. The first one is derived starting from the premise that the accuracy of the delay estimate should be prioritized over the accuracy of the DOA estimate because the delay accuracy directly influences the precision of GNSS pseudo-range observable. The second approach relies on the assumption that the accuracy of the DOA estimates is to prioritize because the DOA is needed to create a beamformer that can mitigate spoofing or multipath. The last approach focuses on obtaining both accurate DOA and delay estimates. In accordance with these different requirements, we come up with a series of joint spatial domain and temporal domain sparse models where on-grid and off-grid models are adopted.

Let $\tilde{\theta} \doteq [\tilde{\theta}_1, \dots, \tilde{\theta}_{N_\theta}]$ be the uniformly fixed sampling spatial grids with fixed DOA interval r_θ in the range $[-90^\circ, 90^\circ]$. Similarly, let $\tilde{\tau} \doteq [\tilde{\tau}_1, \dots, \tilde{\tau}_{N_\tau}]$ be the uniformly fixed sampling time grids with fixed delay interval r_τ in the range $[-2T_c, 2T_c]$ where T_c denotes the time duration per C/A code. Thus, we can construct an on-grid DOA and delay basis matrix

$$\Phi = A \otimes C \tag{7}$$

where the (m_θ, n_θ) element of $A \in \mathbb{C}^{M_\theta \times N_\theta}$ is $C \in \mathbb{C}^{M_\tau \times N_\tau}$, the m_θ^{th} element of the steering vector $a(\tilde{\theta}_{n_\theta})$ with $m_\theta = 1, \dots, M_\theta, n_\theta = 1, \dots, N_\theta$, and the (m_τ, n_τ) element of $C \in \mathbb{C}^{M_\tau \times N_\tau}$ is $r(\tilde{\tau}_{m_\tau}, \tilde{\tau}_{n_\tau})$ with $m_\tau = 1, \dots, M_\tau, n_\tau = 1, \dots, N_\tau$.

The off-grid delay vector, $\beta_\tau \doteq [\beta_1, \dots, \beta_{N_\tau}]^T$ contains the components $\beta_{n_\tau} \doteq \tau_k - \tilde{\tau}_{n_\tau, k}$, which are assumed to be uniformly distributed in the interval $[-\frac{1}{2}r_\tau, \frac{1}{2}r_\tau]$ with $\tilde{\tau}_{n_\tau, k}$ being the nearest grid point to the k^{th} signal. We can construct an on-grid DOA and off-grid delay basis matrix as

$$\Phi_{\beta_\tau} = A \otimes (C + B_\tau \text{diag}(\beta_\tau)) \tag{8}$$

where $B_\tau \in \mathbb{C}^{M_\tau \times N_\tau}$ is the first-order derivative of C with respect to $\tilde{\tau}_{n_\tau}$, which is composed of $b_\tau(\tilde{\tau}_{m_\tau}, \tilde{\tau}_{n_\tau})$ with $n_\tau = 1, \dots, N_\tau, m_\tau = 1, \dots, M_\tau$ and $b_\tau(\tilde{\tau}_{m_\tau}, \tilde{\tau}_{n_\tau}) \doteq \frac{\partial r(\tilde{\tau}_{m_\tau}, \tilde{\tau}_{n_\tau})}{\partial \tilde{\tau}_{n_\tau}}$.

Similarly, for off-grid DOA vector $\beta_\theta \doteq [\beta_1, \dots, \beta_{N_\theta}]^T$, it is formed by $\beta_{n_\theta} = \theta_k - \tilde{\theta}_{n_\theta, k}$, which are assumed to be uniformly distributed in the interval $[-\frac{1}{2}r_\theta, \frac{1}{2}r_\theta]$, with each $\tilde{\theta}_{n_\theta, k}$ being the nearest grid point to the k^{th} signal. Thus, an

on-grid DOA and off-grid delay basis matrix can be represented as

$$\Phi_{\beta_\theta} = (A + B_\theta \text{diag}(\beta_\theta)) \otimes C \tag{9}$$

where $B_\theta \in \mathbb{C}^{M_\theta \times N_\theta}$ is the first-order derivative of A with respect to $\tilde{\theta}_{n_\theta}$, which is composed of $b_\theta(m_\theta, \tilde{\theta}_{n_\theta})$ with $m_\theta = 1, \dots, M_\theta, n_\theta = 1, \dots, N_\theta$ and $b_\theta(m_\theta, \tilde{\theta}_{n_\theta}) = \frac{\partial a(m_\theta, \tilde{\theta}_{n_\theta})}{\partial \tilde{\theta}_{n_\theta}}$.

We extend the above single measurement vector to multiple, specifically N , measurement vectors as $Y \doteq [y_s(1), \dots, y_s(N)] \in \mathbb{C}^{M_\theta M_\tau \times N}$ and $E \doteq [e_s(1), \dots, e_s(N)] \in \mathbb{C}^{M_\theta M_\tau \times N}$. Then, the joint on-grid DOA and on-grid delay estimation sparse model is given by

$$Y = \Phi X + E \tag{10}$$

with complex source amplitudes matrix $X \doteq [x_s(1), \dots, x_s(N)] \in \mathbb{C}^{N_\theta N_\tau \times N}$ where X is row sparse since only a few entries of X are nonzero, and they tend to appear in the same positions in each column. In (10), Φ can be replaced by either (8) or (9) to represent the other two models, which can be expressed as

$$Y = \Phi_{\beta_\tau} X + E \tag{11}$$

$$Y = \Phi_{\beta_\theta} X + E \tag{12}$$

Equations (11) and (12) are the joint on-grid DOA and off-grid delay and joint off-grid DOA and on-grid delay sparse model, respectively.

Joint angle and delay estimation based on multiple sparse Bayesian learning

The three different signal models lead to three different methods: the JAODE-MSBL providing more accurate delay estimates, the JOADE-MSBL for more precise DOA estimates, and the JADE-MSBL&SAGE providing both accurate DOA and delay estimates. JAODE-MSBL is described first, and the other two algorithms are outlined later.

Joint on-grid angle and off-grid delay estimation based on multiple sparse Bayesian learning

The problem of joint on-grid DOA and off-grid delay estimation consists in finding not only the set of nonzero indices of X but also the off-grid shifts β_τ for the delays. An algorithm based on the MSBL methodology is presented below.

Likelihood and prior

Given that the additive noise \mathbf{E} in (11) is assumed to be complex Gaussian with mean value zero and variance σ^2 , the data likelihood for the sources \mathbf{X} given the observations \mathbf{Y} is complex Gaussian as

$$p(\mathbf{Y}|\mathbf{X}, \lambda_n, \boldsymbol{\beta}_\tau) = \prod_{n=1}^N \mathcal{CN}(\mathbf{y}_s(n) | \boldsymbol{\Phi}_{\boldsymbol{\beta}_\tau} \mathbf{x}_s(n), \lambda_n^{-1} \mathbf{I}_{M_\theta M_\tau}) \quad (13)$$

A Gamma hyperprior (since it is a conjugate prior of the Gaussian distribution) is adopted for the unknown precision, $\lambda_n \triangleq \sigma^{-2}$, and it can be expressed as

$$p(\lambda_n; a, b) = \mathcal{B}(\lambda_n | a, b) \quad (14)$$

with the hyperparameters a and b , and $\mathcal{B}(\lambda_n | a, b) \triangleq [\Gamma(a)]^{-1} b^a \lambda_n^{a-1} e^{-b\lambda_n}$ being $\Gamma(a) = \int_0^\infty x^{a-1} e^{-x} dx$ the Gamma function.

For the prior of \mathbf{X} , we assume that columns are uncorrelated between them and each one follows a zero-mean complex Gaussian distribution with DOA-delay-dependent variance $\boldsymbol{\alpha} = [\alpha_1, \dots, \alpha_{N_\theta N_\tau}]^T$ and $\mathbf{Y} = \text{diag}(\boldsymbol{\alpha})$,

$$p(\mathbf{X}|\boldsymbol{\alpha}) = \prod_{n=1}^N \mathcal{CN}(\mathbf{x}_s(n) | 0, \mathbf{Y}) \quad (15)$$

A two-stage hierarchical prior: $p(\mathbf{X}; \rho) = \int p(\mathbf{X}|\boldsymbol{\alpha}) p(\boldsymbol{\alpha}; \rho) d\boldsymbol{\alpha}$ is adopted with hyperparameter $\rho > 0$

$$p(\boldsymbol{\alpha}; \rho) = \prod_{n_g=1}^{N_\theta N_\tau} \mathcal{B}(\boldsymbol{\alpha}(n_g) | 1, \rho) \quad (16)$$

which promotes the row sparsity of \mathbf{X} , that is to say, it favors that most rows of \mathbf{X} are zero.

For the off-grid parameter vector $\boldsymbol{\beta}_\tau$, a non-informative uniform prior is used

$$p(\boldsymbol{\beta}_\tau; r_\tau) = U\left(-\frac{1}{2}r_\tau, \frac{1}{2}r_\tau\right) \quad (17)$$

where we have

$$U(c, d) = \begin{cases} \frac{1}{d-c}, & c \leq x \leq d \\ 0, & \text{otherwise} \end{cases} \quad (18)$$

To estimate DOA and delay, we can formulate the following problem to maximize the posterior probability given the received signal

$$\{\hat{\mathbf{X}}, \hat{\lambda}_n, \hat{\boldsymbol{\alpha}}, \hat{\boldsymbol{\beta}}_\tau\} = \arg \max_{\{\mathbf{X}, \lambda_n, \boldsymbol{\alpha}, \boldsymbol{\beta}_\tau\}} p(\mathbf{X}, \lambda_n, \boldsymbol{\alpha}, \boldsymbol{\beta}_\tau | \mathbf{Y}) \quad (19)$$

The problem of posterior probability above cannot be solved directly; hence, the expectation maximization (EM) method is applied to MSBL. By combining the stages of the hierarchical Bayesian model, the joint probability density function (PDF) is

$$p(\mathbf{X}, \mathbf{Y}, \lambda_n, \boldsymbol{\alpha}, \boldsymbol{\beta}_\tau) = p(\mathbf{Y}|\mathbf{X}, \lambda_n, \boldsymbol{\beta}_\tau) p(\mathbf{X}|\boldsymbol{\alpha}) p(\boldsymbol{\alpha}) p(\lambda_n) p(\boldsymbol{\beta}_\tau) \quad (20)$$

with the distributions on the right-hand side as defined by (13), (15), (16), (14) and (17), respectively.

Posterior

Given the likelihood of the array observations (13), and the priors (15) and (16), the posterior PDF for the source amplitudes \mathbf{X} can be found using the Bayes rule conditioned on λ_n and $\boldsymbol{\alpha}$ as

$$p(\mathbf{X}|\mathbf{Y}; \lambda_n, \boldsymbol{\alpha}, \boldsymbol{\beta}_\tau) \propto p(\mathbf{Y}|\mathbf{X}; \lambda_n, \boldsymbol{\beta}_\tau) p(\mathbf{X}; \rho) \quad (21)$$

It is easy to show that the posterior distribution of \mathbf{X} is a complex Gaussian distribution, since both $p(\mathbf{Y}|\mathbf{X}; \lambda_n, \boldsymbol{\beta}_\tau)$ and $p(\mathbf{X}; \rho)$ are Gaussians, with posterior mean $\boldsymbol{\mu}$ and covariance $\boldsymbol{\Sigma}$

$$\begin{aligned} \boldsymbol{\mu}(n) &= E\{\mathbf{x}_s(n) | \mathbf{Y}, \lambda_n, \boldsymbol{\alpha}, \boldsymbol{\beta}_\tau\} \\ &= \lambda_n \boldsymbol{\Sigma} \boldsymbol{\Phi}_{\boldsymbol{\beta}_\tau}^H \mathbf{y}_s(n) \end{aligned} \quad (22)$$

$$\begin{aligned} \boldsymbol{\Sigma} &= E\left\{(\mathbf{x}_s(n) - \boldsymbol{\mu}(n))(\mathbf{x}_s(n) - \boldsymbol{\mu}(n))^H | \mathbf{Y}, \lambda_n, \boldsymbol{\alpha}, \boldsymbol{\beta}_\tau\right\} \\ &= \left(\lambda_n \boldsymbol{\Phi}_{\boldsymbol{\beta}_\tau}^H \boldsymbol{\Phi}_{\boldsymbol{\beta}_\tau} + \mathbf{Y}^{-1}\right)^{-1} \end{aligned} \quad (23)$$

where $n = 1, \dots, N$. The Woodbury matrix identity can be applied to obtain $\boldsymbol{\Sigma} = \mathbf{Y} - \mathbf{Y} \boldsymbol{\Phi}_{\boldsymbol{\beta}_\tau}^H \boldsymbol{\Sigma}_y^{-1} \boldsymbol{\Phi}_{\boldsymbol{\beta}_\tau} \mathbf{Y}$, where the array data covariance $\boldsymbol{\Sigma}_y$ is

$$\boldsymbol{\Sigma}_y = E\{\mathbf{y}_s(n) \mathbf{y}_s^H(n)\} = \lambda_n^{-1} \mathbf{I} + \boldsymbol{\Phi}_{\boldsymbol{\beta}_\tau} \mathbf{Y} \boldsymbol{\Phi}_{\boldsymbol{\beta}_\tau}^H \quad (24)$$

which is derived from (6).

Expectation and maximization

From the formulations mentioned above, hyperparameters $\lambda_n, \boldsymbol{\alpha}, \boldsymbol{\beta}_\tau$ are needed to be known to calculate $\boldsymbol{\mu}$ and $\boldsymbol{\Sigma}$. To address the estimation of hyperparameters, an EM algorithm is implemented. It treats \mathbf{X} as a hidden variable and turns to maximizing $E\{p(\mathbf{X}, \mathbf{Y}, \lambda_n, \boldsymbol{\alpha}, \boldsymbol{\beta}_\tau)\}$ with respect to each hyperparameter. Following a similar procedure as Tipping (2001) described, denoting $\mathbf{U} = [\boldsymbol{\mu}(1), \dots, \boldsymbol{\mu}(N)]$, it is easy to obtain the following updates of λ_n and $\boldsymbol{\alpha}$ by maximizing

$E\{\ln p(\mathbf{Y}|\mathbf{X}, \lambda_n, \boldsymbol{\alpha}, \boldsymbol{\beta}_\tau) p(\lambda_n)\}$ and $E\{\ln p(\mathbf{X}|\boldsymbol{\alpha}) p(\boldsymbol{\alpha})\}$, respectively

$$\lambda_n = \frac{M_\theta M_\tau N + a - 1}{E\left\{\left\|\mathbf{Y} - \boldsymbol{\Phi}_{\beta_\tau} \mathbf{X}\right\|_F^2\right\} N + b} \tag{25}$$

$$\alpha(n_g) = \frac{\sqrt{N^2 + 4\rho E\left\{\left\|\mathbf{X}(n_g, :)\right\|_2^2\right\}} - 1}{2\rho} \tag{26}$$

where $E\left\{\left\|\mathbf{Y} - \boldsymbol{\Phi}_{\beta_\tau} \mathbf{X}\right\|_F^2\right\} = \left\|\mathbf{Y} - \boldsymbol{\Phi}_{\beta_\tau} \mathbf{U}\right\|_F^2 + \alpha(n_g) \sum_{n=1}^{N_\theta N_\tau} \zeta(n_g)$ with $\zeta(n_g) = 1 - \alpha^{-1}(n_g) \boldsymbol{\Sigma}(n_g, n_g)$, and $E\left\{\left\|\mathbf{X}(n_g, :)\right\|_2^2\right\} = \left\|\mathbf{U}(n_g, :)\right\|_2^2 + \boldsymbol{\Sigma}(n_g, n_g)$ with $n_g = 1, \dots, N_\theta N_\tau$.

As for the off-grid vector $\boldsymbol{\beta}_\tau$, we can obtain the following likelihood function by maximizing $E\{\log p(\mathbf{Y}|\mathbf{X}, \lambda_n, \boldsymbol{\alpha}, \boldsymbol{\beta}_\tau) p(\boldsymbol{\beta}_\tau)\}$, what results in the following expression after ignoring the terms independent of $\boldsymbol{\beta}_\tau$:

$$\begin{aligned} & E\left\{\frac{1}{N} \sum_{n=1}^N \left\|\mathbf{y}_s(n) - \boldsymbol{\Phi}_{\beta_\tau} \mathbf{x}_s(n)\right\|_2^2\right\} \\ &= \frac{1}{N} \sum_{n=1}^N \left\|\mathbf{y}_s(n) - \boldsymbol{\Phi}_{\beta_\tau} \boldsymbol{\mu}(n)\right\|_2^2 + \text{Tr}\left\{\boldsymbol{\Phi}_{\beta_\tau} \boldsymbol{\Sigma} \boldsymbol{\Phi}_{\beta_\tau}^H\right\} \\ &= \boldsymbol{\beta}_\tau^T \mathbf{P}_\tau \boldsymbol{\beta}_\tau - 2\mathbf{v}_\tau^T \boldsymbol{\beta}_\tau + C_1 \end{aligned} \tag{27}$$

where C_1 is a constant term independent of $\boldsymbol{\beta}_\tau$, \mathbf{P}_τ is a positive semi-definite matrix

$$\begin{aligned} \mathbf{P}_\tau &= \Re\left\{\frac{1}{N} \sum_{n=1}^N \boldsymbol{\Xi}_\tau^H \boldsymbol{\Xi}_\tau\right\} + \\ & \Re\left\{\mathbf{J}_{N_\theta N_\tau \times N_\tau}^T \left(\boldsymbol{\Sigma} \odot (\mathbf{A} \otimes \mathbf{B}_\tau)^H (\mathbf{A} \otimes \mathbf{B}_\tau)\right) \mathbf{J}_{N_\theta N_\tau \times N_\tau}\right\} \end{aligned} \tag{28}$$

$$\begin{aligned} \mathbf{v}_\tau &= \Re\left\{\frac{1}{N} \sum_{n=1}^N \left\{\left(\mathbf{y}_s(n) - (\mathbf{A} \otimes \mathbf{C}) \boldsymbol{\mu}(n)\right)^H \boldsymbol{\Xi}_\tau\right\}\right\}^T \\ & - \Re\left\{\left\{\text{diag}\left((\mathbf{A} \otimes \mathbf{B}_\tau)^H (\mathbf{A} \otimes \mathbf{C}) \boldsymbol{\Sigma}\right)\right\}^T \mathbf{J}_{N_\theta N_\tau \times N_\tau}\right\}^T \end{aligned} \tag{29}$$

with $\boldsymbol{\Xi}_\tau = ((\mathbf{A} \cdot \text{mat} \boldsymbol{\mu}^T(n)) \otimes \mathbf{I}_{M_\tau})(\mathbf{I}_{N_\tau} \otimes \mathbf{B}_\tau) \mathbf{J}_{N_\tau \times N_\tau}$ and $\text{mat} \boldsymbol{\mu}(n) \in \mathbb{C}^{N_\theta \times N_\tau}$ being a reshaped matrix of $\boldsymbol{\mu}(n)$. $\mathbf{J}_{N_\theta N_\tau \times N_\tau}$ is defined by $\mathbf{J}_{N_\theta N_\tau \times N_\tau} \doteq \mathbf{1}_{N_\theta} \otimes \mathbf{I}_{N_\tau}$. $\mathbf{J}_{N_\tau \times N_\tau}$ is with the element of $(N_\tau(m_\tau - 1) + m_\tau)$ row and m_τ column being one, $m_\tau = 1, \dots, N_\tau$, and other elements being zero. Besides, the detailed derivation of (27)-(29) is shown in Appendix.

For the purpose of estimating $\boldsymbol{\beta}_\tau$, we have

$$\hat{\boldsymbol{\beta}}_\tau = \arg \min_{\boldsymbol{\beta}_\tau \in \left[-\frac{1}{2}r_\tau, \frac{1}{2}r_\tau\right]} \left\{\boldsymbol{\beta}_\tau^T \mathbf{P}_\tau \boldsymbol{\beta}_\tau - 2\mathbf{v}_\tau^T \boldsymbol{\beta}_\tau\right\} \tag{30}$$

To simplify the above calculation, by (30) and $\frac{\partial}{\partial \boldsymbol{\beta}_\tau} \left\{\boldsymbol{\beta}_\tau^T \mathbf{P}_\tau \boldsymbol{\beta}_\tau - 2\mathbf{v}_\tau^T \boldsymbol{\beta}_\tau\right\} = 2(\mathbf{P}_\tau \boldsymbol{\beta}_\tau - \mathbf{v}_\tau)$ we have $\hat{\boldsymbol{\beta}}_\tau = \mathbf{P}_\tau^{-1} \mathbf{v}_\tau$ in case of \mathbf{P}_τ being invertible.

After describing in detail the derivation of the JAODE-MSBL method, we sketch how the other estimators are obtained since the derivation follows similar steps to the previous ones, so we highlight only the differences.

Joint off-grid angle and on-grid delay estimation based on multiple sparse Bayesian learning

Following the sparse model (9) and (12) for JOADE-MSBL, the solutions of λ_n and $\boldsymbol{\alpha}$ can be obtained by adopting the same steps of (25) and (26). We can compute the off-grid DOA estimate vector $\boldsymbol{\beta}_\theta$ following the same procedure described in (27)-(30) with the corresponding changes in the expressions:

$$\begin{aligned} & E\left\{\frac{1}{N} \sum_{n=1}^N \left\|\mathbf{y}_s(n) - \boldsymbol{\Phi}_{\beta_\theta} \mathbf{x}_s(n)\right\|_2^2\right\} \\ &= \frac{1}{N} \sum_{n=1}^N \left\|\mathbf{y}_s(n) - \boldsymbol{\Phi}_{\beta_\theta} \boldsymbol{\mu}(n)\right\|_2^2 + \text{Tr}\left\{\boldsymbol{\Phi}_{\beta_\theta} \boldsymbol{\Sigma} \boldsymbol{\Phi}_{\beta_\theta}^H\right\} \\ &= \boldsymbol{\beta}_\theta^T \mathbf{P}_\theta \boldsymbol{\beta}_\theta - 2\mathbf{v}_\theta^T \boldsymbol{\beta}_\theta + C_2 \end{aligned} \tag{31}$$

with the matrix \mathbf{P}_θ and the vector \mathbf{v}_θ given by

$$\begin{aligned} \mathbf{P}_\tau &= \Re\left\{\frac{1}{N} \sum_{n=1}^N \boldsymbol{\Xi}_\tau^H \boldsymbol{\Xi}_\tau\right\} + \\ & \Re\left\{\mathbf{J}_{N_\theta N_\tau \times N_\tau}^T \left(\boldsymbol{\Sigma} \odot (\mathbf{A} \otimes \mathbf{B}_\tau)^H (\mathbf{A} \otimes \mathbf{B}_\tau)\right) \mathbf{J}_{N_\theta N_\tau \times N_\tau}\right\} \end{aligned} \tag{32}$$

$$\begin{aligned} \mathbf{v}_\theta &= \Re\left\{\frac{1}{N} \sum_{n=1}^N \left\{\left(\mathbf{y}_s(n) - (\mathbf{A} \otimes \mathbf{C}) \boldsymbol{\mu}(n)\right)^H \boldsymbol{\Xi}_\theta\right\}\right\} \\ & - \Re\left\{\left\{\text{diag}\left((\mathbf{B}_\theta \otimes \mathbf{C})^H (\mathbf{A} \otimes \mathbf{C}) \boldsymbol{\Sigma}\right)\right\}^T \mathbf{J}_{N_\theta N_\tau \times N_\tau}\right\} \end{aligned} \tag{33}$$

In the above formulation, $\boldsymbol{\Xi}_\theta = (\mathbf{B}_\theta \otimes \mathbf{I}_{M_\tau})(\mathbf{I}_{N_\theta} \otimes (\mathbf{C} \cdot \text{mat} \boldsymbol{\mu}(n))) \mathbf{J}_{N_\theta^2 \times N_\theta} \cdot \mathbf{J}_{N_\theta N_\tau \times N_\theta}$ is defined by $\mathbf{J}_{N_\theta N_\tau \times N_\theta} \doteq [\mathbf{O}_{N_\tau \times N_\theta}(1), \dots, \mathbf{O}_{N_\tau \times N_\theta}(N_\theta)]^T$, and the n_θ^{th} matrix $\mathbf{O}_{N_\tau \times N_\theta}(n_\theta)$ is with the n_θ^{th} column being one and the other entries being zeros. $\mathbf{J}_{N_\theta^2 \times N_\theta}$ is with the element of $(N_\theta(m_\theta - 1) + m_\theta)$ row and m_θ^{th} column being one where $m_\theta = 1, \dots, N_\theta$ and other entries being zero. The JAODE-MSBL and JOADE-MSBL algorithms are summarized in Table 1.

Table 1 JAODE-MSBL and JOADE-MSBL algorithms to estimate the DOAs and delays

	Initialization $\alpha, \lambda_n, \beta_\tau$ or β_θ
	Repeat
1	Calculate μ, Σ and Φ_{β_τ} or Φ_{β_θ} using the current values of the hyperparameters according to (22), (23), (24), and (8) or (9), respectively;
2	Update λ_n and α according to (25) and (26) with the sparse model Φ_{β_τ} or Φ_{β_θ} ;
3	Find K the largest peaks in α and calculate the corresponding DOAs and delays grid numbers, respectively;
4	Update β_θ or β_θ according to (27), (28) and (29) or (33), (34) and (35);
5	Calculate the error $\varepsilon = \ \alpha^{new} - \alpha^{old}\ _2^2 / \ \alpha^{old}\ _2^2$
	Until (convergence)

Joint on-grid angle and on-grid delay estimation based on multiple sparse Bayesian learning and sage

Thanks to the robustness against correlated multipath, JAODE-MSBL and JOADE-MSBL are powerful methods to obtain either accurate delay or DOA estimates. However, high resolution in both DOA and delay may be needed in specific GNSS use cases. The SAGE algorithm provides a way to achieve super-resolution and unbiased estimates, but it has the drawback that it only guarantees local optimality, which makes it extremely sensitive to initial values. Therefore, a combination of SAGE and JADE-MSBL is proposed whereby JADE-MSBL provides with SAGE the precise initialization values; meanwhile, SAGE returns the finer estimates.

As Fleury (1999) described, the basic concepts of SAGE are the hidden data space breaking down the multi-dimensional optimization problem into several smaller ones, and the parameter estimation for each path by sequentially conditioning on a subset of parameters while keeping the parameters of the complement subset fixed.

According to model (2), we introduce a definition of $s_k(t) \doteq \gamma_k \mathbf{a}(\theta_k) c(t - \tau_k) e^{j2\pi\delta_k t}$ with $d(t) = e^{j2\pi\delta_k t}$. After collecting N code periods and we get

$$Y_N = [y(1), \dots, y(L), \dots, y((N - 1)L + 1), \dots, y((N - 1)L + L)] \in \mathbb{C}^{M_\theta \times LN} \tag{34}$$

and $S_{N,k} \in \mathbb{C}^{M_\theta \times LN}$, $E_{N,k} \in \mathbb{C}^{M_\theta \times LN}$, $\mathbf{c}_N(\tau_k) \in \mathbb{C}^{1 \times LN}$ and $\mathbf{d}_N(\delta_k) \in \mathbb{C}^{1 \times LN}$. The stochastic mapping of the hidden data space to the observed signal is $Y_N = X_{N,k} + \sum_{k'=1, k' \neq k}^K (S_{N,k'} + E_{N,k'})$ where $X_{N,k} \doteq S_{N,k} + E_{N,k}$. After estimating the hidden data space in the so-called expectation step (E-step) with

$$\hat{X}_{N,k} = Y_N - \sum_{k'=1, k' \neq k}^K \hat{S}_{N,k'} \tag{35}$$

where $S_{N,k} = \mathbf{a}(\theta_k) \gamma_k (\mathbf{c}_N(\tau_k) \odot \mathbf{d}_N(\delta_k))$. The maximization step (M-step) is used to estimate in each hidden data space

$$z(\theta_k, \tau_k, \delta_k) = \mathbf{a}^H(\theta_k) \hat{X}_{N,k} (\mathbf{c}_N(\tau_k) \odot \mathbf{d}_N(\delta_k))^H \tag{36}$$

$$\hat{\theta}_k = \arg \max_{\theta_k} \left\{ |z(\theta_k, \hat{\tau}_k, \hat{\delta}_k)|^2 \right\} \tag{37}$$

$$\hat{\tau}_k = \arg \max_{\tau_k} \left\{ |z(\hat{\theta}_k, \tau_k, \hat{\delta}_k)|^2 \right\} \tag{38}$$

$$\hat{\delta}_k = \arg \max_{\delta_k} \left\{ |z(\hat{\theta}_k, \hat{\tau}_k, \delta_k)|^2 \right\} \tag{39}$$

$$\hat{\gamma}_k = \frac{z(\hat{\theta}_k, \hat{\tau}_k, \hat{\delta}_k)}{M_\theta LN} \tag{40}$$

which are performed. Obviously, the estimated hidden data space in (35) is the vulnerable step that requires precise estimates to ensure the correct path elimination, and these estimates can be the on-grid estimated DOAs and delays obtained with JADE-MSBL. The JADE-MSBL&SAGE algorithm is outlined in Table 2.

While the number of iterations required by the three proposed algorithms to achieve the root mean square error (RMSE) floor depends on the situation, and in particular, on the correlation between signals, a relatively low number of iterations between 10 and 25 suffices.

Table 2 JADE-MSBL&SAGE algorithm to estimate the DOAs and delays

	Initialization α, α_n
	Repeat
1	Calculate μ, Σ and Φ using the current values of the hyperparameters according to (22), (23), (24) and (7) respectively;
2	Update λ_n and α according to (25) and (26) with the sparse model; Φ
3	Find the K largest peaks in and α calculate the corresponding DOAs and delays grid numbers, respectively;
4	Calculate the error $\varepsilon = \ \alpha^{new} - \alpha^{old}\ _2^2 / \ \alpha^{old}\ _2^2$
	Until (convergence)
5	Initialize SAGE with the estimated DOAs and delays from JADE-MSBL;
6	Search for the finer DOAs, delays, FFOs and amplitudes sequentially in a small range with each hidden data space according to (35), (36) (37), (38), (39) and (40)

Numerical results

This section investigates the performance of JAODE-MSBL, JOADE-MSBL, JADE-MSBL&SAGE, SAGE and spatial smoothing-JADE-MUSIC (SS-JADE-MUSIC) for various GNSS multipath cases.

For all the proposed approaches based on sparse representation, the scanning DOA grid is uniformly distributed in the range from -90° to 90° with DOA interval of $r_\theta = 2^\circ$ between adjacent grid points. Likewise, we use a uniform scanning delay grid range from $-2T_c$ to $2T_c$, with delay interval $r_\tau = 0.1T_c$. As for the initialization, we set $\rho = 0.01$ and $a = b = 1 \times 10^{-4}$. In addition, λ_n and α are initialized as $\lambda_n = \frac{100}{var\{Y}}$ with $var\{Y\}$ denoting as the element-wise variance of Y and $\alpha = \frac{1}{M_\theta M_\tau N} \sum_{n=1}^N |\Phi^H y_s(n)|$. Off-grid vectors are set as $\beta_\tau = \mathbf{0}$ or $\beta_\theta = \mathbf{0}$. The convergence condition is satisfied with $\varepsilon \leq 10^{-3}$ or the number of iterations exceeding 500.

Unless noted otherwise, SAGE is implemented by two different initializations: the ideal one (SAGEi) and the practical one (SAGEp). The former is that both DOAs and delays are initialized in a uniformly random way within a very range around the true value of the parameters. The ranges for the DOA and delay are $(-\frac{3}{4}r_\theta, \frac{3}{4}r_\theta)$ and $(-\frac{3}{4}r_\tau, \frac{3}{4}r_\tau)$, respectively. To account for a more realistic environment, in SAGEp the initial DOAs are unknown and the initial delays are constrained to be in a $[-2T_c, 2T_c]$ range centered on the true delay, since in practice a rough estimation of the delay is available thanks to the acquisition step. For comparison purposes, two-dimensional (2D) SAGE for DOA and delay is applied to all cases, and the 3D-SAGE for DOA, delay and FFO is used in the cases C and D, as described below.

JADE-MUSIC subspace method is implemented as described in Vanderveen et al (1997) and Chang et al (2018). Spatial smoothing with 6 sliding elements and forward averaging are adopted to facilitate the decorrelation of the multipaths and the LOS.

Before presenting our results, there are some settings needed to be explicitly stated. We assume a uniform linear array with $M_\theta = 8$ sensors and half-wavelength interelement spacing. We use $N = 10$ periods of C/A codes in total, so the total duration of the observed signals is 10 ms. The sample interval is $T_s = \frac{1}{P}T_c$ where the sample rate P is 4 and T_c is the duration of each chip in one C/A code period, that is $T_c = \frac{1}{1023}$ ms. We consider two paths $K = 2$ in total: the LOS signal (LOSS) and a single reflective multipath. The two paths are in phase, which means $\arg(\gamma_1) = \arg(\gamma_2)$, and the direct-to-multipath ratio is $|\gamma_1|/|\gamma_2| = 0.8$.

In this analysis, RMSE is averaged over $N_l = 1000$ Monte Carlo realizations for each C/N_0 point, and the RMSE is

$$\text{defined as } \text{RMSE}(\tau) \doteq \sqrt{\frac{1}{KN_l} \sum_{n_l=1}^{N_l} \sum_{k=1}^K (\hat{\tau}_k - \tau_k)^2}$$
, with similar

expressions for $\text{RMSE}(\theta)$ and $\text{RMSE}(\delta)$. The relevant Cramér-Rao lower bounds are computed referring to Antreich et al (2008) and Seco Granados (2000).

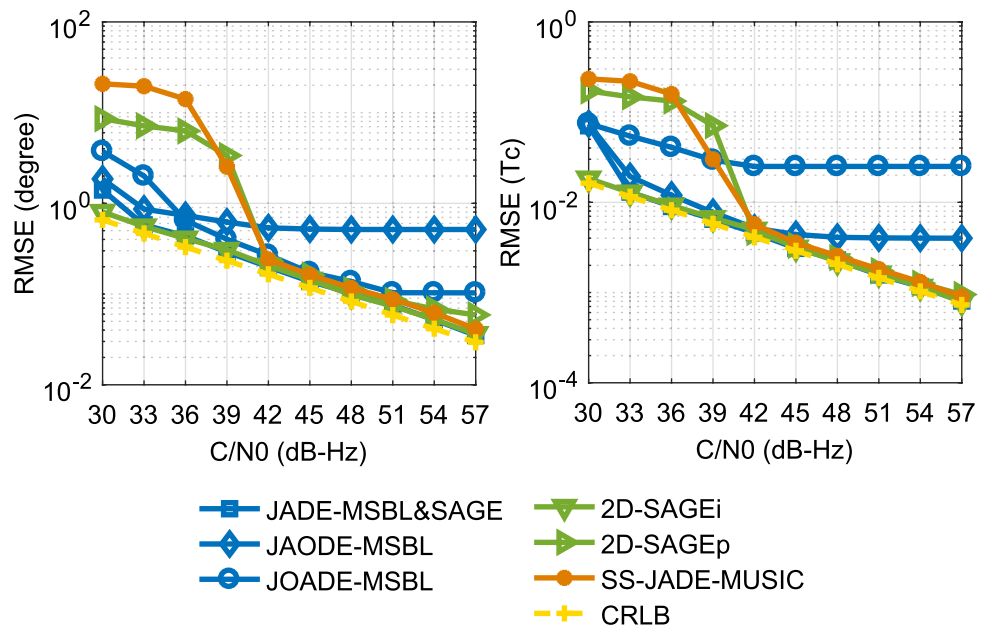
– *Case A Temporally correlated rays*

In this case, we consider the LOSS and the multipath signal are separable in spatial domain. These two correlated rays impinge from DOAs θ_1 and θ_2 equal to -0.7° and 30.2° , and the corresponding delays τ_1 and τ_2 are $0.03T_c$ and $0.38T_c$. The FFOs of both LOSS and multipath signal are assumed zero, $\delta_k = 0, k = 1, \dots, K$.

Figure 1 compares the RMSEs of the three proposed algorithms, 2D-SAGE, SS-JADE-MUSIC and the CRLB as a function of the C/N_0 under the separable DOAs case. As expected, 2D-SAGEi performs well thanks to the help of the exact initialization. In addition, both of 2D-SAGEp and SS-JADE-MUSIC are strongly degraded at moderate and low C/N_0 values.

For the proposed algorithms, the low and inaccurate C/N_0 region is narrowed down to only 3 dB-Hz wide from 30 dB-Hz to 33 dB-Hz. Then, two estimations of on-grid one and off-grid one begin to show a differ-

Fig. 1 RMSEs of the DOAs (left panel) and the delays (right panel) for case A



ence. For the DOA of JAODE-MSBL and the delay of JOADE-MSBL, the off-grid effects become evident when C/N_0 is greater than 42 dB-Hz which means that even if C/N_0 increases, the residual biases are determined by the granularity of the grid, namely $\frac{1}{2}r_\theta$ or $\frac{1}{2}r_\tau$. In contrast, the DOA of JOADE-MSBL and delay of JAODE-MSBL adopting off-grid estimation outperform 2D-SAGEp and SS-JADE-MUSIC. Nevertheless, the performance of off-grid estimation reaches an error floor in high C/N_0 because of the first-order Taylor series expansions. Since JADE-MSBL provides accurate on-grid estimations and SAGE further refines the results, JADE-MSBL&SAGE has more precision than the other proposed algorithms at the price of increased complexity. In general, these simulation results show that our proposed methods are more appropriate than the existing one in the range of typical C/N_0 values for the GNSS signals, that is from 35 dB-Hz to 50 dB-Hz.

– *Case B* Both spatially and temporally correlated rays

In order to gain deeper insight into the performance of the proposed algorithms in both spatially and temporally correlated case, the DOAs θ_1 and θ_2 of the LOSS and the multipath signal are set to 0.3° and 6.8° , while the delays τ_1 and τ_2 remain $0.03T_c$ and $0.38T_c$, respectively. This means that the angular difference between the two rays is less than half of the first beamwidth of the antenna array, and the delay difference is less than half a chip. The FFOs are the same as case A.

Figure 2 results confirm that it is difficult to resolve the two paths if the angle and delay difference are both close enough unless the C/N_0 is high enough. Worse still, 2D-SAGEp can hardly distinguish the paths in any case.

2D-SAGEi always behaves good but the RMSE reaches a floor level at high C/N_0 .

JADE-MSBL-based algorithms show strong robustness to multipath. In spite of the fact that JAODE-MSBL and JOADE-MSBL also experience an error floor in the DOA and delay RMSEs, respectively, both of them behave well, especially from 30 dB-Hz to 48 dB-Hz. In particular, as far as the delay estimate is concerned, JAODE-MSBL performs as good as 2D-SAGEi, even reaching the $10^{-2}T_c$ level, which corresponds to a decimeter error level in the pseudo-range at 42 dB-Hz. Moreover, JADE-MSBL&SAGE provides more reliable estimates, what means that the on-grid initial estimates obtained with JADE-MSBL are more accurate than the idealistic initialization values assumed in 2D-SAGEi.

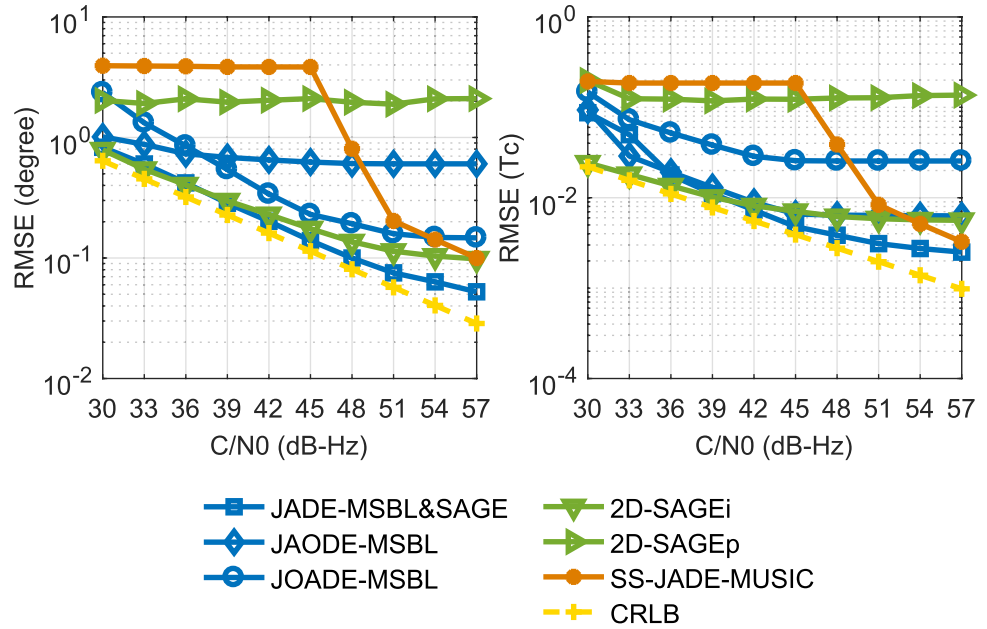
– *Case C* Both spatially and temporally correlated rays within FFOs.

Under the situation of DFOs completely compensated, the proposed algorithms indeed perform well no matter how spatially and temporally correlated the rays are. However, in practice, DFOs of each path are neither identical nor completely compensated, and hence, some FFOs remain to be estimated. In Case C, we consider FFOs within ± 500 Hz, and we analyze the performance and the robustness against FFOs.

First, we use the same settings as in case B, but adding to each path an FFO of $\delta_1 = 400$ Hz and $\delta_2 = -300$ Hz, respectively.

As can be seen in Fig. 2, 3 D-SAGEi loses its resolvable ability due to the lack of FFO estimation step. This phenomenon also happens in 3D-SAGEp, but the reason is the inaccurate initialization. On the other hand,

Fig. 2 RMSEs of the DOAs (left panel) and the delays (right panel) for case B



3D-SAGEi performs very well and the initial FFOs values are very accurate and different among them. Besides, as the large FFO difference between the LOSS and the multipath signal improves the resolution, SS-JADE-MUSIC performs better than that in case B but still suffers a clear degradation at low C/N_0 . On the contrary, although JOADE-MSBL and JAODE-MSBL only perform a 2D estimation, both of them have almost the same performance as that in case B, which stands out their robustness to FFOs. Moreover, unlike in case B, JADE-MSBL&SAGE no longer tends flat to be flat at

high C/N_0 , but it is close to CRLB since the large FFO difference decreases the similarity of the two paths.

For the sake of testing the discrimination of the LOSS and the multipath signal within small FFO difference, here we change the FFOs to $\delta_1 = 400\text{Hz}$ and $\delta_2 = 380\text{Hz}$, respectively.

In contrast to the case C with separable FFOs, the closer the FFOs are, the harder it is to resolve the two paths as shown in Fig. 4. The most obvious limitation is experienced by SS-JADE-MUSIC, which does not obtain moderately accurate estimates until around 50 dB-Hz.

Fig. 3 RMSEs of the DOAs (left panel) and the delays (right panel) for case C with large difference of FFOs

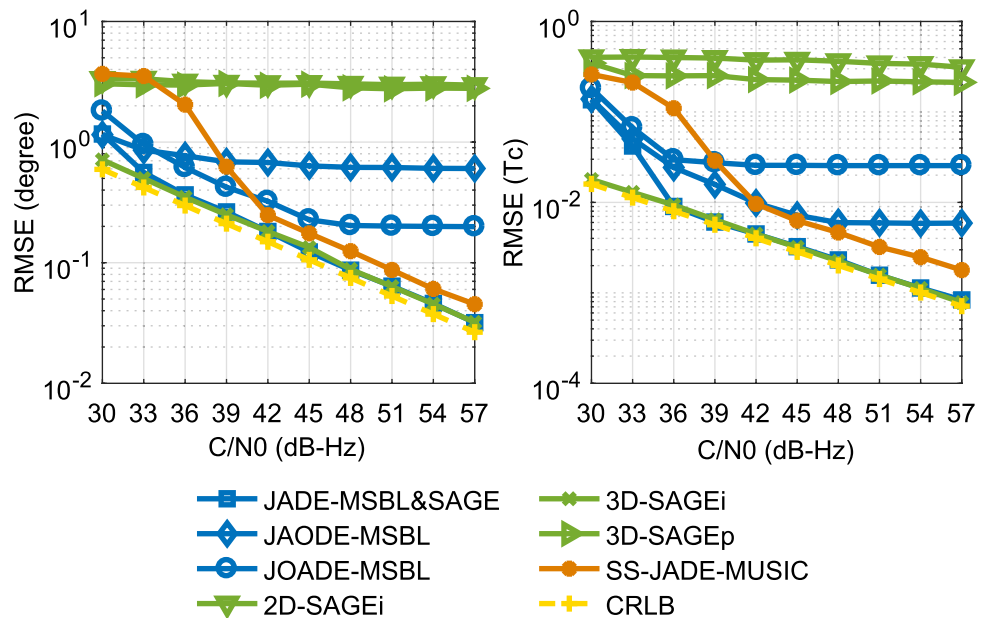


Fig. 4 RMSEs of the DOAs (left panel) and the delays (right panel) for case C with a small difference of FFOs

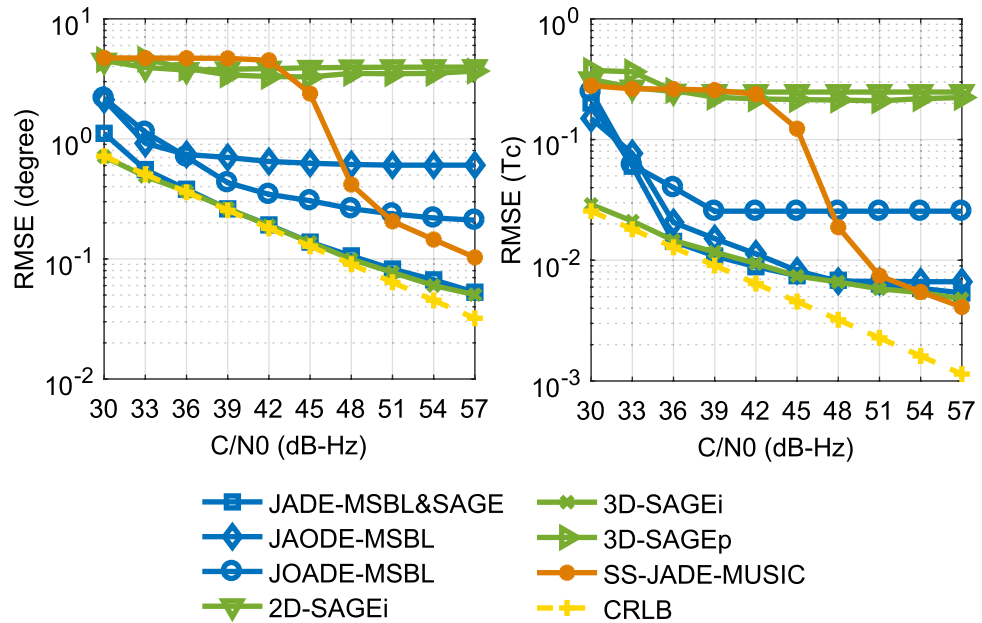
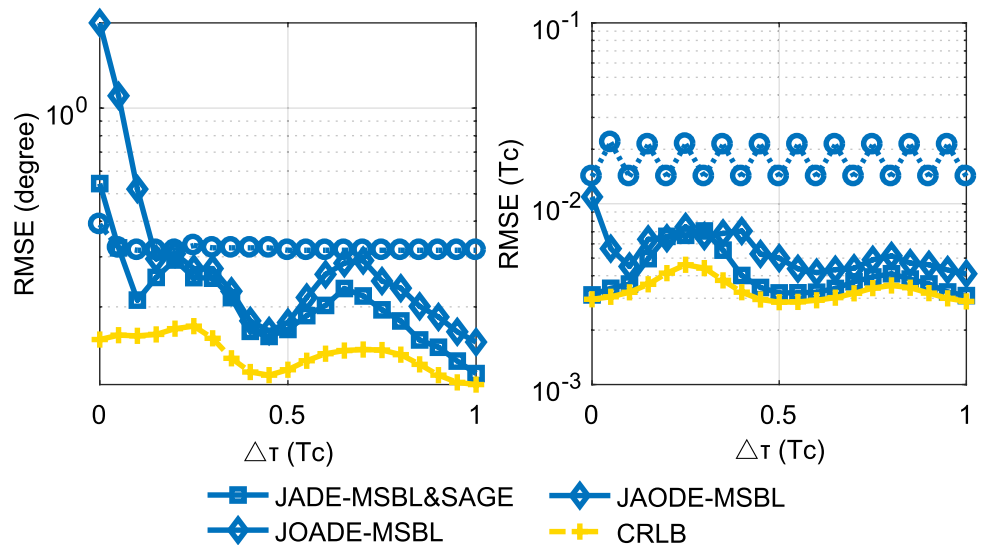


Fig. 5 RMSEs of the DOAs (left panel) and the delays (right panel) for case D as a function of $\Delta\tau$



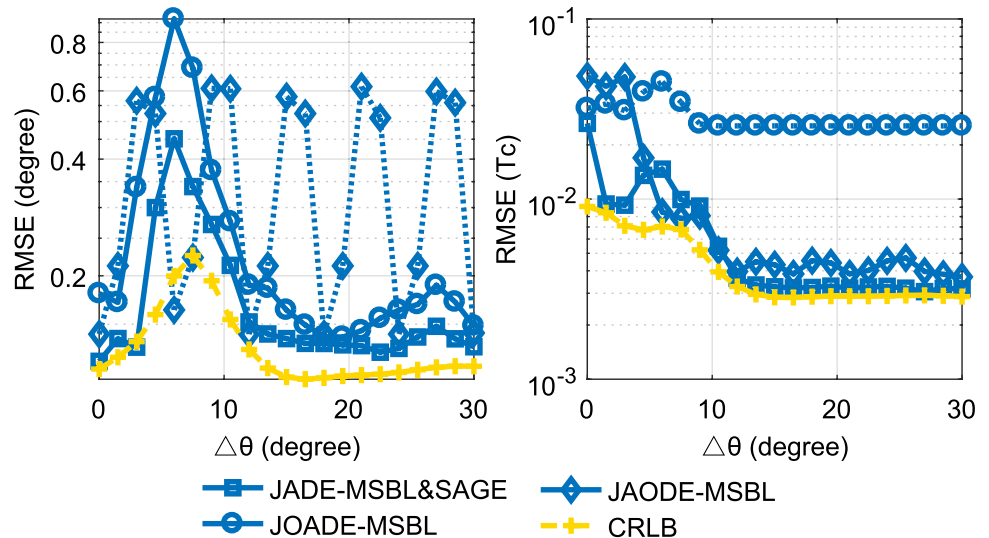
Moreover, 2D-SAGEi and 3D-SAGEp still perform poorly. It is worth remarking that the delay estimation accuracy of JADE-MSBL&SAGE remains almost constant above 45 dB-Hz, remaining basically the same as that of 3D-SAGEi. This is because it is difficult to distinguish the two paths when they have similar DOAs, delays and FFOs simultaneously.

- *Case D* the RMSEs via varied DOA or delay difference
 - All the cases above consider fixed DOAs and delays. In this case, we study the performances as a function of the delay or the DOA differences.
 - In case D, the DOAs θ_1 and θ_2 are set to 0.2° and 10.2° . This means that the DOA difference is smaller than the

first beamwidth of the array. The delay difference is denoted as $\Delta\tau \doteq |\tau_1 - \tau_2|$, ranging from 0 to $1T_c$, and the C/N_0 is 45 dB-Hz.

Figure 5 illustrates the RMSEs of DOAs and delays as a function of the relative delay. All the proposed algorithms follow the trend of CRLBs except, as expected, the JAODE-MSBL for DOA and JOADE-MSBL for a delay due to the on-grid estimation. The irregular behaviors of the CRLB are due to the very small DOA difference between the rays. It is worth noting that in general JADE-MSBL&SAGE is much closer to the CRLB than JAODE-MSBL does in delay and JOADE-MSBL does in DOA. Only for some points of $\Delta\tau$ around $0.25T_c$ the RMSE of

Fig. 6 RMSEs of the DOAs (left panel) and the delays (right panel) for case D as a function of $\Delta\theta$



JADE-MSBL&SAGE is slightly above JAODE-MSBL. This occurs because SAGE suffer sometimes from poor separation capability of highly correlated rays.

Next, we consider another case with two temporally correlated rays with a delay difference of $0.25T_c$ while the DOA difference $\Delta\theta \doteq |\theta_1 - \theta_2|$ varies from 0° to 30° and the C/N_0 is 45 dB-Hz.

Figure 6 presents the RMSEs of DOA and delay as a function of the relative DOA. As expected, in general, the error decreases as the relative DOA increases. In Fig. 6, the RMSEs of JAODE-MSBL and JADE-MSBL&SAGE become very close to the CRLB when the two DOAs are non-spatially separable. The delay RMSE of JOADE-MSBL remains constant because of the grid granularity. In contrast, the DOA RMSE of both JOADE-MSBL and JADE-MSBL&SAGE follows the CRLB, while JAODE-MSBL has some specific errors in the very particular cases when the true values of DOA coincide with the grid points.

Conclusion

We have investigated the joint DOA and delay estimation problem in a GNSS multipath environment. The MBSL method, possibly with off-grid extensions, has been applied to jointly estimate DOA and delay for GNSS multipath signals. The off-grid and on-grid estimation have also been considered concurrently. Thus either a more accurate delay estimation algorithm (JAODE-MSBL) or a more precise DOA estimate algorithm (JOADE-MSBL) have been proposed for different GNSS practical applications. Additionally, as an alternative to off-grid estimation, we have proposed the algorithm JADE-MSBL&SAGE,

whereby SAGE takes advantage of the initial values to refine the estimates. Our simulation results confirm that the three proposed algorithms can well handle the discrimination and estimation of the multipath signals and perform significantly better than the present methods in some severe cases, especially at low C/N_0 and with both spatially and temporally correlated rays. Such good characteristics can be attributed to the robustness of JADE-MSBL in front of multipath and low C/N_0 conditions, and also to the resolution enhancement provided by off-grid estimation. The linear approximation used in off-grid estimation produces an error floor happened only at very high C/N_0 values.

Appendix

We calculate (27) through the following two equalities where the sampling point is omitted for short:

$$\begin{aligned} & \|y_s - \Phi_{\beta_\tau} \mu\|_2^2 \\ &= \|y_s - (A \otimes C) \mu - \Xi_\tau \beta_\tau\|_2^2 \\ &= \beta_\tau^T \Xi_\tau^H \Xi_\tau \beta_\tau - 2\Re\left\{ (y_s - (A \otimes C) \mu)^H \Xi_\tau \right\} \beta_\tau + C_1 \end{aligned} \tag{41}$$

$$\begin{aligned} & Tr\left\{ \Phi_{\beta_\tau} \Sigma \Phi_{\beta_\tau}^H \right\} \\ &= 2\Re\left\{ Tr\left\{ (A \otimes C) \Sigma (A \otimes (B_\tau \text{diag}(\beta_\tau)))^H \right\} \right\} \\ &+ Tr\left\{ (A \otimes (B_\tau \text{diag}(\beta_\tau))) \Sigma (A \otimes (B_\tau \text{diag}(\beta_\tau)))^H \right\} + C_2 \end{aligned} \tag{42}$$

where C_1 and C_2 are the parts irrelevant to β_τ . Equation (42) can be obtained by the following two parts:

$$\begin{aligned} & \Re \left\{ \text{Tr} \left\{ (A \otimes C) \Sigma (A \otimes (B_\tau \text{diag}(\beta_\tau)))^H \right\} \right\} \\ &= \Re \left\{ \text{Tr} \left\{ (A \otimes C) \Sigma \left[\text{diag} (J_{N_\theta N_\tau \times N_\tau} \beta_\tau) (A^H \otimes B_\tau^H) \right] \right\} \right\} \quad (43) \\ &= \Re \left\{ \text{diag} \left((A^H A \otimes B_\tau^H C) \Sigma \right) \right\}^T (J_{N_\theta N_\tau \times N_\tau} \beta_\tau) \end{aligned}$$

$$\begin{aligned} & \text{Tr} \left\{ (A \otimes (B_\tau \text{diag}(\beta_\tau))) \Sigma (A \otimes (B_\tau \text{diag}(\beta_\tau)))^H \right\} \\ &= \text{Tr} \left\{ \left((A \otimes B_\tau) \text{diag} (J_{N_\theta N_\tau \times N_\tau} \beta_\tau) \right) \right. \\ & \quad \left. \Sigma \left(\text{diag} (J_{N_\theta N_\tau \times N_\tau} \beta_\tau) (A^H \otimes B_\tau^H) \right) \right\} \quad (44) \\ &= \beta_\tau^T J_{N_\theta N_\tau \times N_\tau}^T \left(\Sigma \odot (A \otimes B_\tau) \right)^H (A \otimes B_\tau) J_{N_\theta N_\tau \times N_\tau} \beta_\tau \end{aligned}$$

Note that $\beta_\tau^T Q \beta_\tau$ belongs to real domain under the circumstance of a positive semi-definite matrix Q and thus leads to a result $\beta_\tau^T Q \beta_\tau = \Re \{ \beta_\tau^T Q \beta_\tau \} = \beta_\tau^T \Re \{ Q \} \beta_\tau$ due to the real-valued β_τ . Then we have the positive semi-definite matrix P_τ . As for the solution to (31), the derivations can be referred to that of (27).

Acknowledgment The work of G. Seco-Granados was supported in part by the Research and Development Projects of Spanish Ministry of Science, Innovation, and Universities under Grants TEC2017-89925-R and TEC2017-90808-REDT, and by the ICREA Academia Program.

Data Availability Data sharing not applicable to this article as no datasets were generated or analyzed during the current study.

References

- Akaike H (1974) A new look at the statistical model identification. *IEEE Trans Autom Control* 19(6):716–723
- Antreich F, Nossek JA, Utschick W (2008) Maximum likelihood delay estimation in a navigation receiver for aeronautical applications. *Aerosp Sci Technol* 12(3):256–267
- Antreich F, Nossek JA, Seco-Granados G, Swindlehurst AL (2011) The Extended Invariance Principle for Signal Parameter Estimation in an Unknown Spatial Field. *IEEE Trans Signal Process* 59(7):3213–3225
- Avd V, Vanderveen MC, Paulraj AJ (1998) Joint angle and delay estimation using shift-invariance techniques. *IEEE Trans Signal Process* 46(2):405–418
- Chang N, Hong X, Wang W, Wang Z Subspace Based Joint Delay and Direction of Arrival Estimation for GNSS Multipath Signals. In, Singapore, 2018. China Satellite Navigation Conference (CSNC) 2018 Proceedings. Springer Singapore, pp 189–199
- Chen SS, Donoho DL, Saunders MA (2001) Atomic decomposition by basis pursuit. *Siam Review* 43(1):129–159
- Chen P, Cao Z, Chen Z, Wang X (2018) Off-grid DOA estimation using sparse bayesian learning in MIMO radar with unknown mutual coupling. *IEEE Trans Signal Process* 67(1):208–220
- Du L, Yardibi T, Li J, Stoica P (2009) Review of user parameter-free robust adaptive beamforming algorithms. *Digital Signal Process* 19(4):567–582
- Flury BH, Tschudin M, Heddergott R, Dahlhaus D, Pedersen KI (1999) Channel parameter estimation in mobile radio environments using the SAGE algorithm. *IEEE J Sel Areas Commun* 17(3):434–450
- Fohlmeister F, Iliopoulos A, Sgammini M, et al (2017) Dual polarization beamforming algorithm for multipath mitigation in GNSS. *Signal Processing* 138(SEP.):86–97
- Fortunati S, Grasso R, Gini F, Greco MS, LePage K (2014) Single-snapshot DOA estimation by using compressed sensing. *Eurasip Journal on Advances in Signal Processing* 2014(120)
- Gerstoft P, Mecklenbräuker CF, Xenaki A, Nannuru S (2016) Multisnapshot sparse Bayesian learning for DOA. *IEEE Signal Process Lett* 23(10):1469–1473
- Hong X, Chang N, Wang W, Yin Q Subspace-based Joint DOA, Delay and DFO Estimation for GNSS Multipath Signals. Proc. ION GNSS 2018, Institute of Navigation, Miami, Florida, USA, September, 3788–3801
- Irisigler M (2010) Characterization of multipath phase rates in different environments. *GPS Solutions* 14(4):305–317
- Jia Q, Wu R, Wang W, Lu D, Wang L, Li J (2017) Multipath interference mitigation in GNSS via WRELAX. *GPS Solutions* 21(2):487–498
- Juang JC (2008) Multi-objective approach in GNSS code discriminator design. *IEEE Trans Aerosp Electr Syst* 44(2):481–492
- Kalyanaraman SK, Braasch MS, Kelly JM (2006) Code tracking architecture influence on GPS carrier multipath. *IEEE Trans Aerosp Electron Syst* 42(2):548–561
- Kos T, Markezic I, Pokrajcic J Effects of multipath reception on GPS positioning performance. In: Proceedings ELMAR-2010, 15–17 Sept. 2010, pp 399–402
- Li J, Zheng D, Stoica P (1997) Angle and waveform estimation via RELAX. *IEEE Trans Aerosp Electron Syst* 33(3):1077–1087
- Maqsood M, Gao S, Brown T, Unwin M Effects of ground plane on the performance of multipath mitigating antennas for GNSS. In: 2010 Loughborough Antennas & Propagation Conference, 8–9 Nov. 2010, pp 241–244
- Misra P, Enge P (2011) Global Positioning System: signals, measurements and performance. Ganga-Jamuna Press
- O'Brien AJ (2009) Adaptive antenna arrays for precision GNSS receivers. The Ohio State University, Columbus
- Pillai SU, Kwon BH (1989) Forward/backward spatial smoothing techniques for coherent signal identification. *IEEE Trans Acoust Speech Signal Process* 37(1):8–15
- Roy R, Kailath T (1989) ESPRIT-estimation of signal parameters via rotational invariance techniques. *IEEE Trans Acoust Speech Signal Process* 37(7):984–995. <https://doi.org/10.1109/29.32276>
- Schmidt R (1986) Multiple emitter location and signal parameter estimation. *IEEE Trans Antennas Propag* 34(3):276–280
- Seco Granados G (2000) Antenna arrays for multipath and interference mitigation in GNSS receivers. Universitat Politècnica de Catalunya, Barcelona
- Seco Granados G, Fernández Rubio JA, Fernández Prades C (2005) ML estimator and hybrid beamformer for multipath and interference mitigation in GNSS receivers. *IEEE Trans Signal Process* 53(3):1194–1208
- Tibshirani R (1996) Regression shrinkage and selection via the lasso. *J Roy Stat Soc: Ser B (Methodol)* 58(1):267–288
- Tipping ME (2001) Sparse Bayesian learning and the relevance vector machine. *J Mach Learn Res* 1(3):211–244
- Van Nee RDJ (1992) Multipath Effects on GPS Code Phase Measurements. *Navigation* 39:177–190
- Van Nee D, Coenen AJEL (1991) New fast GPS code-acquisition technique using FFT. *Electr Lett* 27:158–160
- Vanderveen MC, Papadias CB, Paulraj A (1997) Joint angle and delay estimation (JADE) for multipath signals arriving at an antenna array. *IEEE Commun Lett* 1(1):12–14
- Wax M, Kailath T (1985) Detection of signals by information theoretic criteria. *IEEE Trans Acoust Speech Signal Process* 33(2):387–392

- Wipf DP, Rao BD (2007) An empirical Bayesian strategy for solving the simultaneous sparse approximation problem. *IEEE Transactions on Signal Processing* 55(7):3704–3716
- Xie P, Petovello MG (2014) Measuring GNSS multipath distributions in urban canyon environments. *IEEE Trans Instrum Meas* 64(2):366–377
- Yang Z, Xie L, Zhang C (2012) Off-grid direction of arrival estimation using sparse Bayesian inference. *IEEE Transactions on Signal Processing* 61(1):38–43
- Yardibi T, Li J, Stoica P, Xue M, Baggeroer AB (2010) Source localization and sensing: A nonparametric iterative adaptive approach based on weighted least squares. *IEEE Trans Aerosp Electron Syst* 46(1):425–443
- Zhang Z, Rao BD (2011) Sparse signal recovery with temporally correlated source vectors using sparse Bayesian learning. *IEEE J Sel Top Signal Process* 5(5):912–926
- Zhu H, Leus G, Giannakis GB (2011) Sparsity-cognizant total least-squares for perturbed compressive sampling. *IEEE Trans Signal Process* 59(5):2002–2016

Publisher's Note Springer Nature remains neutral with regard to jurisdictional claims in published maps and institutional affiliations.



Ning Chang received B.S. and M.S. in communication engineering from Information Engineering University, China, 2011 and Xidian University, China, 2014, respectively. She is currently pursuing the Ph.D. degree in Information and Communication Engineering at Xi'an Jiaotong University. Her research interests include compressed sensing, array signal processing, parameter estimation and multipath mitigation for GNSS signals.



Wenjie Wang received the B.S., M.S., and Ph.D. degrees in information and communication engineering from Xi'an Jiaotong University, Xi'an, China, in 1993, 1998, and 2001, respectively, where he is currently a Professor. His main research interests include information theory, broadband wireless communications, signal processing in communication systems, and array signal processing.



Xi Hong received the B.S. degree in the School of Electronic and Information Engineering, Xi'an Jiaotong University, Xi'an China, in 2012, where he is currently pursuing the Ph.D. degree. His main research interests include array signal processing, signal processing in communication systems, multipath mitigation in navigation, and GNSS physical layer interference detection.



José A. López-Salcedo received his M.Sc. and Ph.D. degrees in Telecommunications Engineering from the Universitat Politècnica de Catalunya, in 2001 and 2007, respectively. In 2006, he joined Universitat Autònoma de Barcelona, where he is an Associate Professor. He held visiting appointments at the University of Illinois Urbana-Champaign, the University of California Irvine, and the European Commission. He is also affiliated with the Institute of Space Studies of Catalonia (IEEC-CERES).



Gonzalo Seco-Granados received the Ph.D. degree in Telecommunications Engineering from the Universitat Politècnica de Catalunya, in 2000, and the MBA degree from IESE Business School, in 2002. Until 2005, he was with the European Space Agency, involved in the design of the Galileo system. Since 2006, he is with Universitat Autònoma de Barcelona and also affiliated with the Institute of Space Studies of Catalonia.